International Journal of Thin Films Science and Technology

http://dx.doi.org/10.18576/ijtfst/150209

Tailoring Structural, Optical and, Electrical Properties of ZnO Spin Coated Films through Boron Doping for Optoelectronic Applications

*Jannatul Fardus Dinar, Shad Afif Sovon and Sinthia Shabnam Mou**

Department of Electrical and Electronic Engineering, University of Rajshahi, Rajshahi-6205, Bangladesh

Received: 10 Jan. 2026, Revised: 12 Feb. 2026, Accepted: 20 Mar. 2026
Published online: 1 May 2026

Abstract: Boron-doped zinc oxide (BZO) thin films were prepared by a low-cost sol–gel spin-coating technique to investigate the influence of boron incorporation on their structural, morphological, optical, and electrical properties. Undoped ZnO and BZO films with 1, 2, 3, and 5 weight percentage (wt%) of boron were synthesized on glass substrates and annealed at 350 °C temperature for 30 min. The films were analyzed using X-ray diffraction (XRD), field emission scanning electron microscopy (FESEM), energy-dispersive X-ray spectroscopy (EDX), UV–Vis spectroscopy, and the van der Pauw technique. The film thickness varied from 30 to 500 nm with increasing boron concentration. XRD confirmed the hexagonal wurtzite structure of undoped ZnO, while boron incorporation reduced the crystallinity. SEM revealed a decrease in grain size and the surface morphology shifted toward an amorphous nature with increasing boron concentration. EDX confirmed the presence of B, Zn, and O in the samples. The optical band gap decreased from 3.31 eV for undoped ZnO to 2.73 eV for 5% BZO. Resistivity increased with B doping and varied non-monotonically from 29.525×10^{-4} to 62.276×10^{-4} $\Omega \cdot$cm for different concentrations of B. The results demonstrate that boron incorporation effectively tunes the properties of ZnO thin films, indicating potential for photovoltaic and optoelectronic applications.

Keywords: Boron-doped ZnO; Sol–gel spin coating; TCO; Optoelectronics; Photovoltaic applications.

1 Introduction

Energy is the key driving force of today's contemporary society and the economic and scientific progress of the society as well as nation depends upon it. The increasing population growth and industrial expansion leading to more energy consumption is driving a rise in energy demand as time goes by [1] and the need for sustainable and environmentally friendly energy sources is increasing. Consequently, renewable energy technologies are receiving increasing global attention. Among the various renewable energy conversion systems, photovoltaic (PV) systems are considered one of the most promising technologies due to their ability to directly convert sunlight into electricity without producing harmful emissions [2, 3].

In PV devices, Transparent conducting oxides (TCO) materials serve as transparent electrodes that simultaneously provide high electrical conductivity and optical transparency, allowing light to reach the active absorber layer while efficiently collecting and transporting charge carriers [4]. Polycrystalline ZnO-based thin films are widely used not only in photovoltaic devices but also in various optoelectronic applications, such as surface acoustic wave devices, chemical sensors, optical detectors and field-effect transistors [4–6]. Unlike many other materials of same applications, ZnO is inexpensive, found in abundance, chemically and thermally stable, easy to synthesize and a non-toxic semiconductor [7]. It has a high exciton binding energy of $\sim$ 60 meV and wide optical band gap of around 3.37 eV at room temperature. ZnO thin films generally show n-type properties with low resistivity due to its oxygen vacancies and zinc interstitials which make them a great pick as TCO [5, 8]. Moreover, ZnO thin films can be adjusted to have higher conductivity, transparency, infrared reflectance and better electron mobility by doping them with convenient dopants, such as the group IIIA elements like Boron (B), Aluminium (Al), Gallium (Ga), and Indium (In) [5, 9, 10].

Boron (B) is the first member of these group IIIA earth metals and because of its high electronegativity and Lewis acid strength it can act as donor when incorporated into the ZnO lattice to contribute extra free electrons, increasing

* Corresponding author e-mail: sinthia.apee@ru.ac.bd

© 2026 NSP
Natural Sciences Publishing Cor.

the carrier concentration as well as conductivity without significantly reducing the optical transmittance [11, 12]. Also, B^{3+} ion has a much shorter cationic radius compared to Zn^{2+} ion and incorporating it in ZnO, in optimized concentrations, could modify the lattice parameters and improve the crystallite growth and reduce certain defects in the film [13, 14]. And of course, boron can be incorporated using inexpensive, abundant precursors like boric acid and its compounds are globally abundant and widely available. These features make Boron-doped ZnO (BZO) an attractive candidate for transparent conducting electrode applications in photovoltaic devices and optoelectronic systems [15].

A variety of deposition techniques have been employed for the fabrication of undoped and boron-doped ZnO thin films, including magnetron sputtering, chemical vapor deposition (CVD), pulsed laser deposition (PLD), spray pyrolysis, and sol–gel spin coating [14]. Among these methods, sol–gel spin coating is particularly attractive because of its simplicity, cost-effectiveness, excellent compositional control, low processing temperature, and ability to coat large areas uniformly without requiring high vacuum systems [10]. These advantages make the sol–gel technique a viable approach for tailoring the physical properties of metal oxide thin films for optoelectronic and photovoltaic applications.

2 Materials and Methods

2.1 Film Preparation

Zinc acetate dihydrate ($Zn(CH_3COO)_2 \cdot 2H_2O$) was selected as the zinc precursor and 2-Methoxyethanol was used as the solvent. Monoethanolamine (MEA) served as the stabilizer. Boric acid (H_3BO_3) was utilized as the boron dopant source. For undoped ZnO film preparation, zinc acetate dihydrate was dissolved in 2-Methoxyethanol to obtain a 0.5 M precursor solution. MEA was subsequently added to the solution such that the molar ratio of MEA to zinc acetate was maintained at 1:1. The mixture was stirred magnetically at 60 °C for 2 h to form a clear and homogeneous solution. For boron doping, boric acid was added to the precursor solution in appropriate amounts to achieve 1, 2, 3, and 5 wt% boron concentrations. The resulting solutions were aged at room temperature for 24 h prior to film deposition.

Microscope glass slides were cut into 2.5×2.5 cm^2 substrates and cleaned sequentially using detergent, acetone, ethanol, and deionized water in an ultrasonic bath for 15 min each, followed by drying in a hot air oven. The aged precursor solution was dispensed onto the cleaned glass substrate and spun at 3000 rpm for 30 s using a spin coater. After each coating cycle, the film was preheated on a hot plate at 150 °C for 10 min to evaporate the solvent and eliminate organic residuals. This procedure was repeated multiple times to achieve the desired film thickness. Finally, the deposited films were annealed in a muffle furnace at 350 °C for 30 min in air atmosphere and allowed to cool slowly to room temperature. A schematic representation of the BZO thin film preparation steps is shown in Fig. 1.

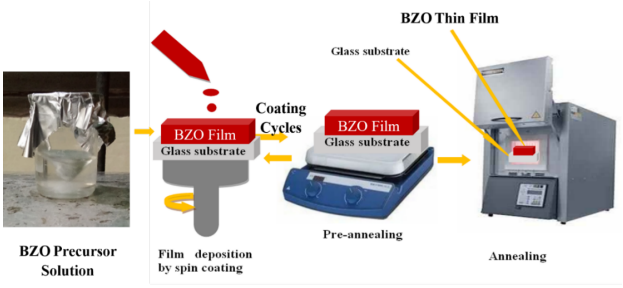


Fig. 1: Steps of BZO film preparation.

2.2 Characterization Techniques

X-ray diffraction (XRD) analysis of the samples was performed using a Rigaku SmartLab SE XRD system with Cu-Kα radiation ($\lambda = 1.5406$ Å) in the 2θ range of 10°–40°. The surface morphology and microstructure of the thin films were examined using Field Emission Scanning Electron Microscopy (FESEM, JEOL JSM-7610F). The elemental composition of the films was analyzed using Energy Dispersive X-ray (EDX) spectroscopy attached to the FESEM system. Film thickness was measured using cross-sectional FESEM imaging and optical profilometry. The optical transmittance and absorbance spectra were recorded using a Shimadzu UV-2600 UV–Vis spectrophotometer in the wavelength range of 300–900 nm. The optical bandgap (E_g) of the films was determined from the Tauc relation:

$$(\alpha h\nu)^n = A(h\nu - E_g), \tag{1}$$

where α denotes the absorption coefficient, $h\nu$ is the incident photon energy, A is an energy-independent constant, and $n = 2$ for direct allowed transitions [16, 17]. The electrical resistivity and conductivity of the prepared thin films were measured at room temperature using the van der Pauw four-probe technique [18].

3 Results and Discussion

3.1 X-ray Diffraction (XRD) Analysis

The XRD patterns of undoped and boron-doped ZnO thin films are shown in Fig. 2. The diffraction peaks of the undoped ZnO film correspond to the (100), (002), and (101) reflection planes, confirming the formation of the hexagonal wurtzite crystal structure (JCPDS card no. 36-1451)

© 2026 NSP
Natural Sciences Publishing Cor.

[18,19]. With the introduction of boron dopant, the diffraction peak intensities decrease significantly, indicating that boron incorporation suppresses crystalline grain growth and promotes an amorphous phase [5]. For 2% BZO, only a broadened (100) peak remains visible, while higher doping levels (3% and 5%) exhibit predominantly amorphous patterns.

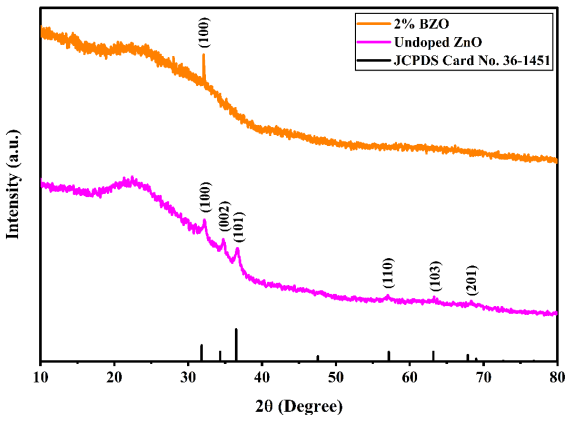


Fig. 2: XRD Spectra of undoped and boron doped ZnO Thin Films.

The structural parameters, including crystallite size (D), micro-strain (ε), and dislocation density (δ), were calculated from the XRD data. The average crystallite size was estimated using Scherrer's formula [20]:

$$D = \frac{0.9\lambda}{\beta \cos\theta}, \tag{2}$$

where β is the full width at half maximum (FWHM) in radians and θ is the Bragg diffraction angle. The micro-strain (ε) and dislocation density (δ) were determined using:

$$\varepsilon = \frac{\beta}{4\tan\theta}, \tag{3}$$

$$\delta = \frac{1}{D^2}. \tag{4}$$

The calculated structural parameters are summarized in Table 1. As the boron concentration increases, the crystallite size decreases while the micro-strain and dislocation density increase, which is attributed to the difference in ionic radii between B^{3+} (0.23 Å) and Zn^{2+} (0.74 Å) and the resulting lattice distortion [21,22].

3.2 Scanning Electron Microscopy (SEM)

The FESEM images (Fig. 3) reveal a clear modification in the surface morphology of the ZnO thin films with increasing boron concentration. The undoped ZnO film exhibits densely packed, well-defined spherical grains with uniform grain distribution. Upon incorporation of 1% B, smaller nanoparticles are formed with reduced grain boundaries. For 2% and 3% BZO, the surface becomes smoother and denser with diminished granularity. At 5% B doping, the film displays a homogeneous, smooth, and compact surface morphology indicative of an amorphous structure, in agreement with the XRD findings [23,24].

Figure 4 shows the cross-sectional FESEM micrographs of undoped, 1%, and 3% BZO thin films. The images confirm good adhesion of the deposited films to the glass substrate without peeling or cracks, with uniform thickness profiles across the substrates.

3.3 Energy Dispersive X-ray (EDX) Spectroscopy

The EDX spectra of the BZO thin films (Fig. 5) confirm the presence of the major constituent elements: zinc (Zn), oxygen (O), and boron (B). The appearance of the boron peak confirms successful incorporation of the dopant into the ZnO host matrix. Trace signals of silicon (Si), sodium (Na), and calcium (Ca) originate from the underlying soda-lime glass substrate [25,26].

3.4 Film Thickness

Figure 6 illustrates the thickness variation of the prepared BZO thin films as a function of boron doping concentration. The film thickness increases with boron content, ranging from approximately 30 nm for undoped ZnO to about 500 nm for 5% BZO. The observed increase in thickness is attributed to the higher solution viscosity and modified sol rheology upon addition of boric acid, which yields thicker layers during the spin-coating deposition process [27].

3.5 Optical Properties

3.5.1 Transmittance and Absorbance

Figure 7(a) shows the optical transmittance spectra of undoped ZnO and BZO thin films in the UV–Vis range (300–900 nm). All films exhibit high optical transparency in the visible wavelength region ($>$ 80%), which satisfies the requirement for transparent conducting oxide applications. A sharp fundamental absorption edge is observed in the near-UV region, corresponding to band-to-band transitions. As the boron doping concentration increases, the absorption edge shifts toward longer wavelengths (red shift), indicating bandgap narrowing.

Figure 7(b) displays the corresponding optical absorbance spectra. The absorbance is low in the visible region and increases sharply at wavelengths below 380 nm

© 2026 NSP
Natural Sciences Publishing Cor.

Table 1: Structural parameter values of ZnO thin films.

Films	Miller Indices (hkl)	Bragg's Angle (°)	Interplanar Spacing d (Å)	FWHM β ($\times 10^{-3}$ rad)	Size D (nm)	Dislocation Density δ ($\times 10^{15}$ m^{-2})	Micro-strain ε ($\times 10^{-3}$)
ZnO	(100)	16.09	2.78	0.42	20.40	2.40	0.364
ZnO	(002)	17.42	2.57	0.73	11.90	7.06	0.581
ZnO	(101)	18.36	2.44	0.55	16.00	3.90	0.414
2% BZO	(100)	16.06	2.78	1.57	91.90	0.11	1.360

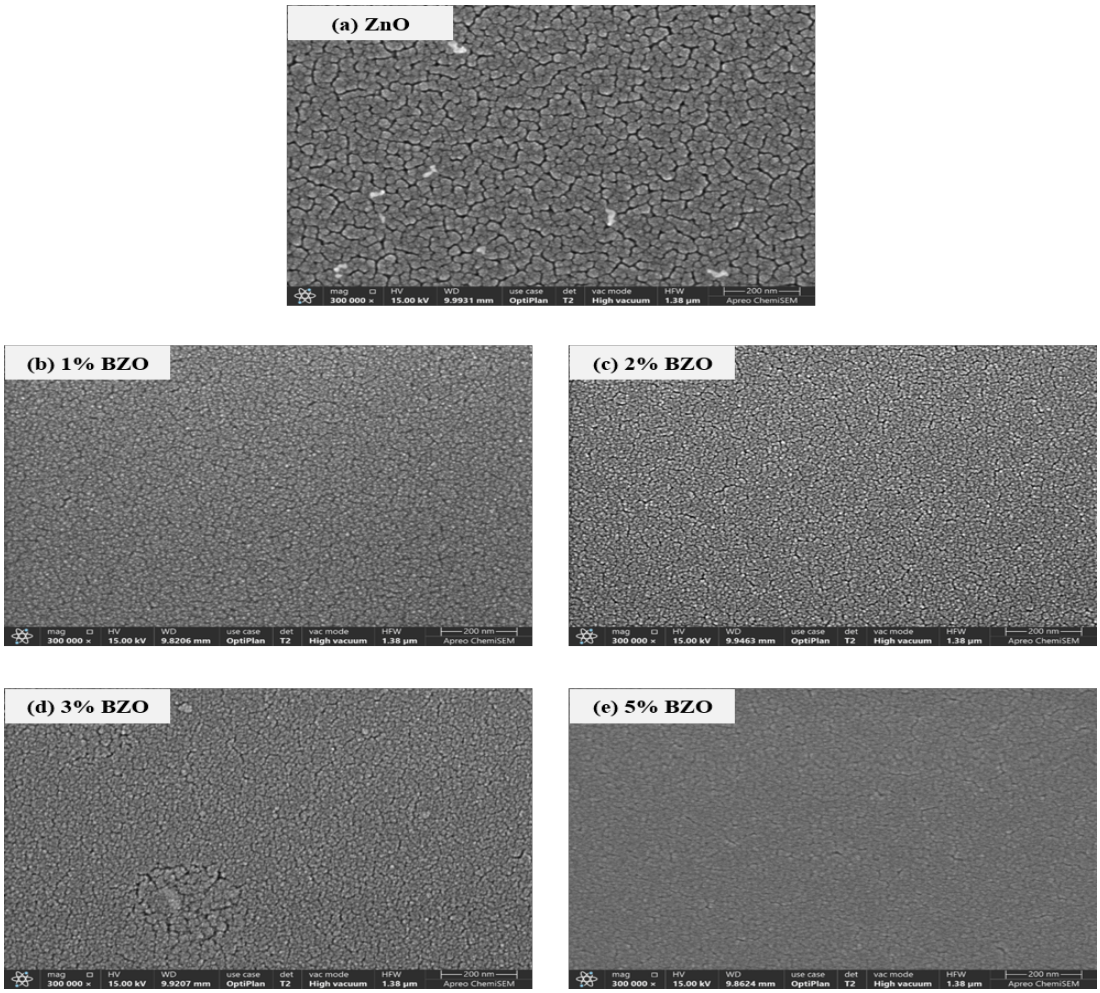


Fig. 3: FESEM Images (300K Magnifications) of (a) undoped ZnO, (b) 1%, (c) 2%, (d) 3%, and (e) 5% BZO Thin Films.

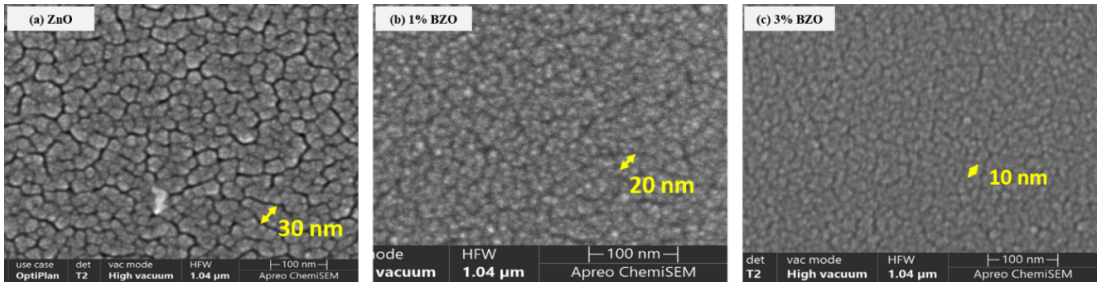
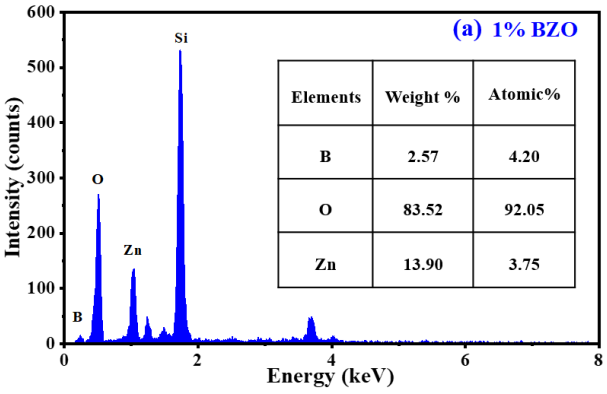
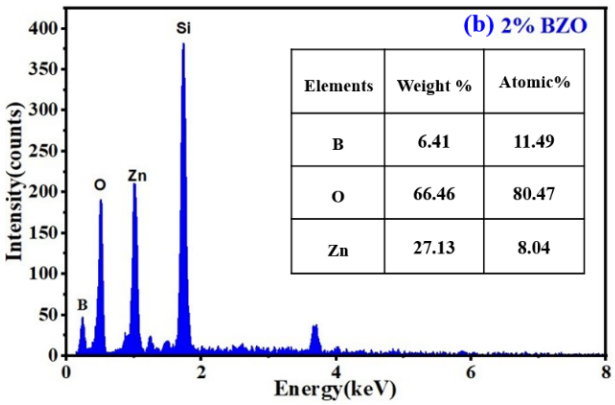


Fig. 4: FESEM images of (a) undoped ZnO, (b) 1%, and (c) 3% thin films showing the variation in film thickness.

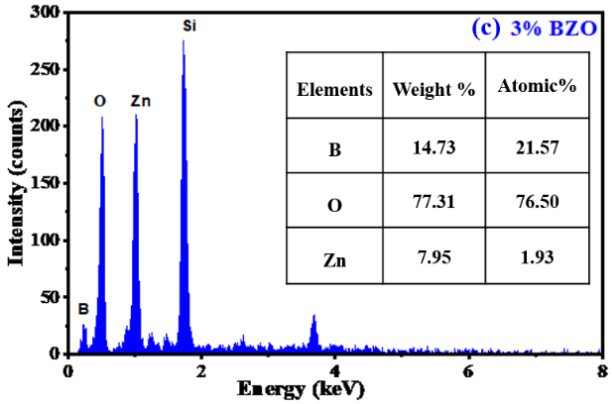
© 2026 NSP
Natural Sciences Publishing Cor.



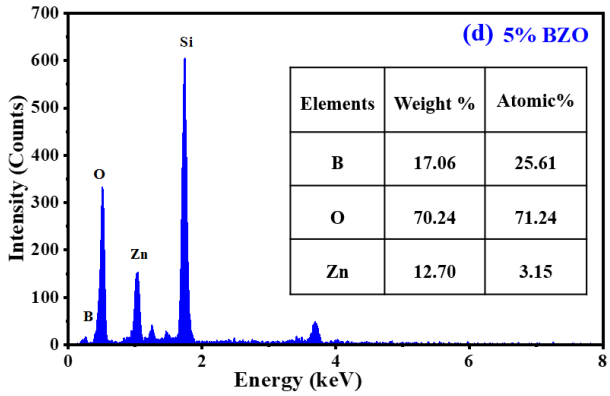
(a) 1% BZO



(b) 2% BZO

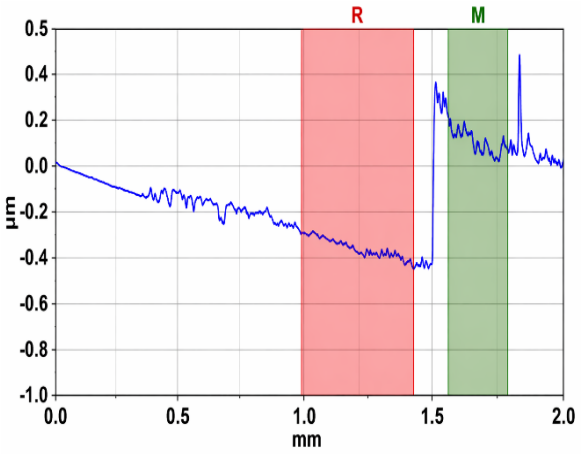


(c) 3% BZO

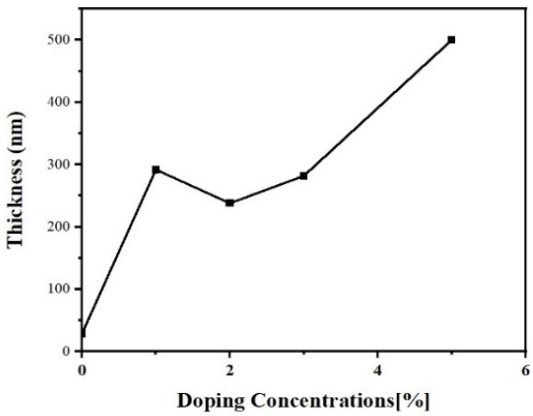


(d) 5% BZO

Fig. 5: EDX Spectra of (a) 1%, (b) 2%, (c) 3%, and (d) 5% BZO thin films.



(a) Thickness of 3% BZO



(b) Thickness variation vs. doping concentration

Fig. 6: (a) Thickness of 3% BZO, and (b) Thickness variation of the BZO thin films with doping concentrations.

© 2026 NSP
Natural Sciences Publishing Cor.

due to electron excitation from the valence band to the conduction band [28].

3.5.2 Optical Bandgap

The optical bandgap (E_g) of the films was determined by extrapolating the linear region of $(\alpha h\nu)^2$ versus photon energy ($h\nu$) plots to $(\alpha h\nu)^2 = 0$, as depicted in Fig. 8. For undoped ZnO, the direct bandgap is found to be 3.31 eV. With increasing boron doping concentration, the bandgap progressively decreases to 3.24 eV (1% BZO), 2.97 eV (2% BZO), 2.88 eV (3% BZO), and 2.73 eV (5% BZO). The bandgap narrowing can be understood in terms of many-body effects, donor-level merging, and structural disorder induced by the incorporation of B^{3+} ions into the ZnO lattice [28, 29].

The optical bandgap values as a function of boron concentration are listed in Table 2 and plotted in Fig. 9.

Table 2: Optical band gap of BZO at different doping concentrations.

Boron doping concentrations [%]	Optical Band Gap [eV]
0	3.31
1	3.24
2	2.97
3	2.88
5	2.73

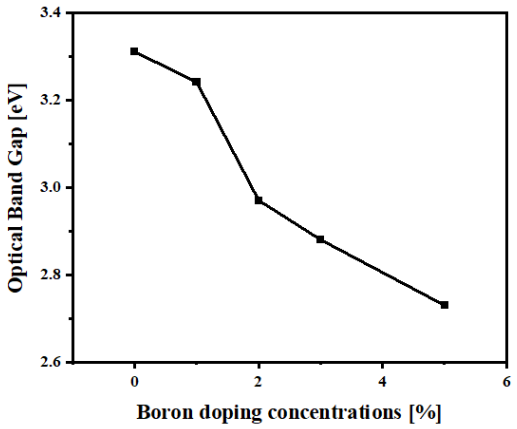


Fig. 9: Optical Band Gap Variations of BZO at different doping concentrations.

3.6 Electrical Properties

The electrical conductivity (σ) and electrical resistivity (ρ) of the prepared ZnO and BZO thin films are illustrated in Fig. 10. The resistivity varies non-monotonically between 29.525×10^{-4} and 62.276×10^{-4} $\Omega \cdot$cm across the investigated doping levels. The minimum resistivity and corresponding highest conductivity are observed at 1% B doping, where effective substitution of Zn^{2+} by B^{3+} releases free electrons and enhances the carrier concentration. At higher doping levels ($> 1\%$), excess boron atoms tend to segregate at grain boundaries or form neutral defect complexes, which act as carrier traps and scattering centers, leading to an increase in resistivity [29, 30].

4 Conclusion

Boron-doped ZnO (BZO) thin films with different boron concentrations (0, 1, 2, 3, and 5 wt%) were successfully prepared on glass substrates via a low-cost sol–gel spin coating technique followed by annealing at 350 °C. XRD analysis confirmed the polycrystalline hexagonal wurtzite structure for undoped ZnO, while boron doping resulted in reduced crystallinity and predominantly amorphous films at higher concentrations. FESEM micrographs showed smooth, compact surfaces with decreasing grain size as boron was incorporated. EDX spectra confirmed the presence of B, Zn, and O throughout the deposited films. Optical characterization revealed high visible transmittance ($> 80\%$) and a systematically decreasing band gap from 3.31 eV (undoped) down to 2.73 eV (5% BZO). Electrical measurements demonstrated optimal electrical conductivity at 1% B doping. These findings demonstrate that boron doping is an effective method for tuning the structural, optical, and electrical properties of spin-coated ZnO thin films, making them promising candidates for photovoltaic devices and transparent conducting electrodes.

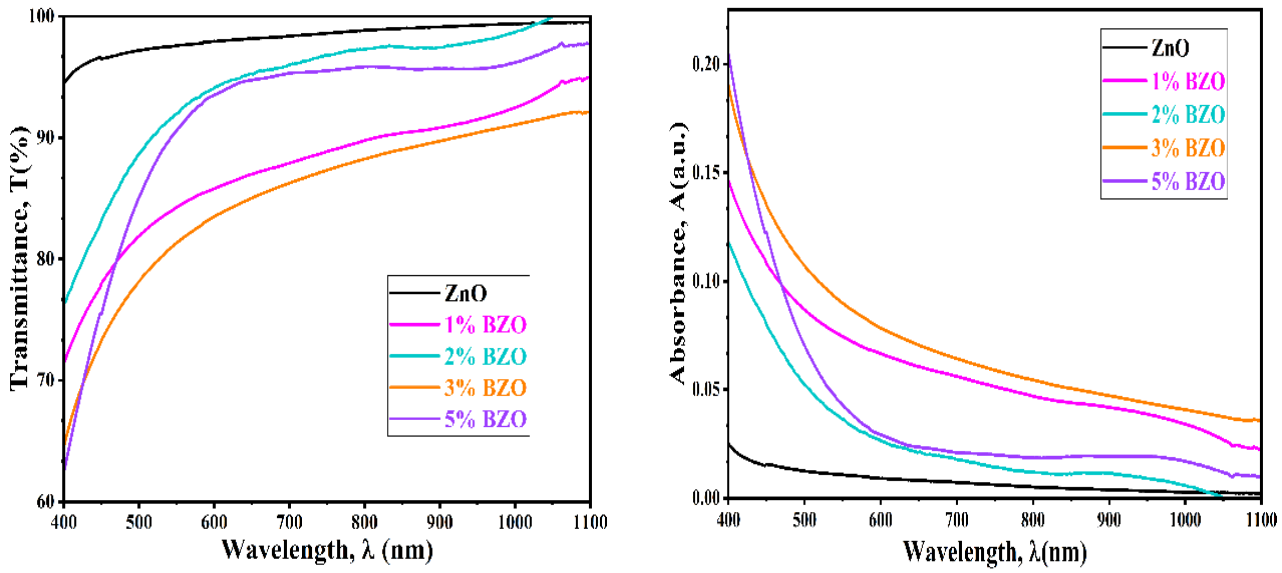
Conflicts of Interest Statement

The authors certify that they have NO affiliations with or involvement in any organization or entity with any financial interest or non-financial interest in the subject matter or materials discussed in this manuscript.

Acknowledgements

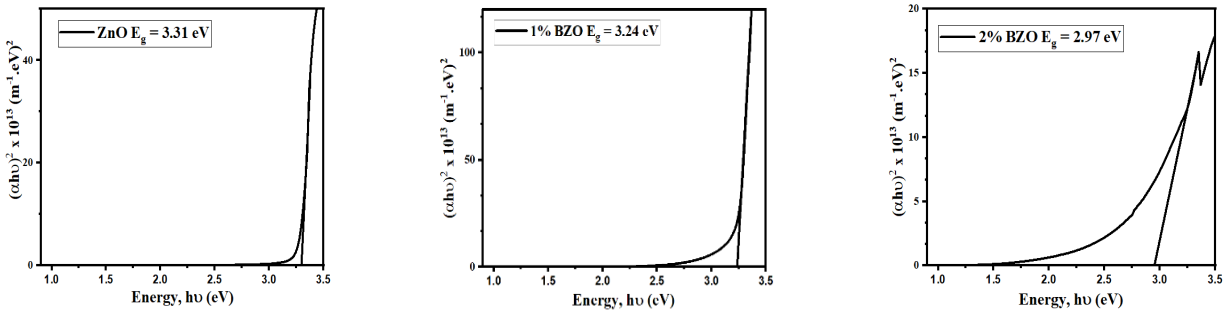
The authors extend their appreciation to the Thin Film Laboratory, Department of Electrical and Electronic Engineering, University of Rajshahi, Rajshahi-6205, Bangladesh, for providing characterization facilities and support.

© 2026 NSP
Natural Sciences Publishing Cor.

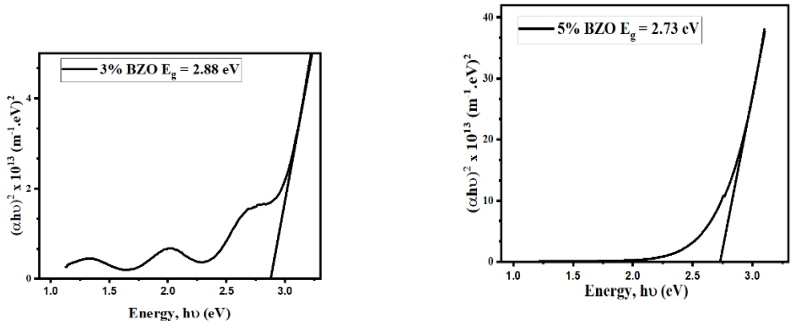


(a) Transmittance (b) Absorbance

Fig. 7: Variation of (a) Transmittance, and (b) Absorbance of different BZO Thin Films.



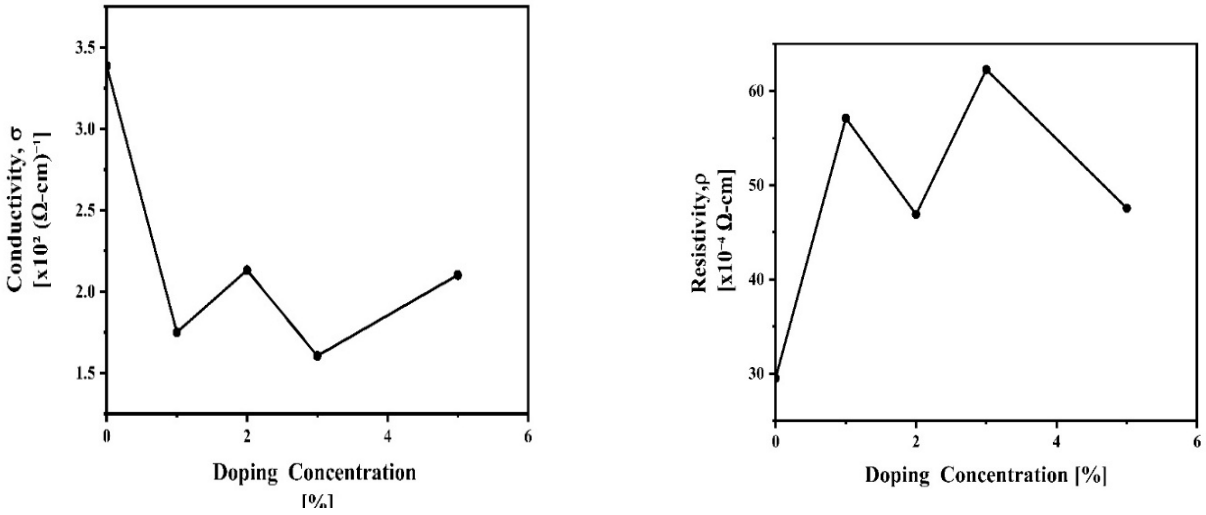
(a) Undoped ZnO (b) 1% BZO (c) 2% BZO



(d) 3% BZO (e) 5% BZO

Fig. 8: Tauc Plot of (a) Undoped ZnO, (b) 1%, (c) 2%, (d) 3% and (e) 5% BZO films.

© 2026 NSP
Natural Sciences Publishing Cor.



(a) Conductivity (b) Resistivity

Fig. 10: Variations in (a) Conductivity, and (b) Resistivity of BZO at different doping concentrations.

References

[1] K.O. Ewansiha, A.O. Ewansiha, C.E. Ewansiha, S.A. Ayo, Zinc Oxide Co-Doped with Aluminium and Boron (Al:B:ZnO) Thin Films via Sol–Gel Process for Solar Cell Window Layers: A Review, Faculty of Natural and Applied Sciences Journal of Applied Chemical Science Research 2 (2025) 16–30.

[2] Y. Li, M. Cheng, E. Jungstedt, B. Xu, L. Sun, L. Berglund, Optically Transparent Wood Substrate for Perovskite Solar Cells, ACS Sustain. Chem. Eng. 7 (2019) 6061–6067.

[3] J. Pastuszak, P. Węgierek, Photovoltaic Cell Generations and Current Research Directions for Their Development, Materials 2022, Vol. 15, Page 5542 15 (2022) 5542.

[4] G.T. Chavan, Y. Kim, M.Q. Khokhar, S.Q. Hussain, E.C. Cho, J. Yi, Z. Ahmad, P. Rosaiah, C.W. Jeon, A Brief Review of Transparent Conducting Oxides (TCO): The Influence of Different Deposition Techniques on the Efficiency of Solar Cells, Nanomaterials 2023, Vol. 13, Page 1226 13 (2023) 1226.

[5] C.Y. Tsay, W.T. Hsu, Sol–gel derived undoped and boron-doped ZnO semiconductor thin films: Preparation and characterization, Ceramics Int. 39 (2013) 7425–7432.

[6] S. Ilican, F. Yakuphanoglu, M. Caglar, Y. Caglar, The role of pH and boron doping on the characteristics of sol gel derived ZnO films, J. Alloys Compd. 509 (2011) 5290–5294.

[7] R. YEASMIN, S.R. BASU, S.S. MOU, SPIN COATED ITO FILMS PREPARED WITH A SOLUTION OF METHANOL: N-PROPYL ALCOHOL (1:1), European Journal of Materials Science and Engineering 5 (2020) 23–31.

[8] A.A. Ahmad, A.M. Alsaad, Q.M. Al-Bataineh, M.A. Al-Naafa, Optical and structural investigations of dip-synthesized boron-doped ZnO-seeded platforms for ZnO nanostructures, Applied Physics A, 2018 124:6 124 (2018) 458-.

[9] L.P. Mwakyusa, N.R. Mlyuka, M.E. Samiji, L.P. Mwakyusa, N.R. Mlyuka, M.E. Samiji, Boron Doped ZnO Films Deposited by DC Reactive Sputtering Using Zn:B Target: Influence of the Deposition Temperature on the Structural, Electrical and Optical Properties, Tanzania Journal of Science 48 (2022) 15.

[10] S.R. Basu, S.S. Mou, Effect of Varying Doping Level on Structural, Electrical and Optical Properties of Al Doped ZnO Spin Coated Films, Adv. Mat. Res. 1171 (2022) 1–10.

[11] J. Hu, R.G. Gordon, Deposition of Boron Doped Zinc Oxide Films and Their Electrical and Optical Properties, J. Electrochem. Soc. 139 (1992) 2014.

[12] S.D. Senol, O. Ozturk, C. Terzioğlu, Effect of boron doping on the structural, optical and electrical properties of ZnO nanoparticles produced by the hydrothermal method, Ceramics Int. 41 (2015) 11194–11201.

[13] S. Jana, A.S. Vuk, A. Mallick, B. Orel, P.K. Biswas, Effect of boron doping on optical properties of sol–gel based nanostructured zinc oxide films on glass, Mater. Res. Bull. 46 (2011) 2392–2397.

[14] B. Wen, C. Liu, W. Fei, H. Wang, S. Liu, N. Wang, W. Chai, Effect of doped boron on the properties of ZnO thin films prepared by sol-gel spin coating, Chemical Research in Chinese Universities 2014 30:3 30 (2014) 509–512.

[15] N. Kati, B. Ayten, Investigation of structural and optical properties of boron-doped ZnO nanomaterials synthesized by hydrothermal method, Journal of the Indian Chemical Society 102 (2025) 101706.

[16] S.A. Sovon, M.H. Khatun, M. Julkarnain, Preparation and characterization of spin-coated Cu2MgSnS4 thin films for photovoltaic applications, Journal of Materials Science: Materials in Electronics 2026 37:11 37 (2026) 824.

© 2026 NSP
Natural Sciences Publishing Cor.

[17] J. Klein, L. Kampermann, B. Mockenhaupt, M. Behrens, J. Strunk, G. Bacher, Limitations of the Tauc Plot Method, Adv. Funct. Mater. 33 (2023) 2304523.
[18] A.M. Alsaad, A.A. Ahmad, I.A. Qattan, Q.M. Al-Bataineh, Z. Albataineh, Structural, Optoelectrical, Linear, and Nonlinear Optical Characterizations of Dip-Synthesized Undoped ZnO and Group III Elements (B, Al, Ga, and In)-Doped ZnO Thin Films, Crystals 2020, Vol. 10, Page 252 10 (2020) 252.
[19] N. Üzar, U. Abdulaziz, Investigation of the effects of coating numbers of thin films and metal contact type on physical properties of undoped ZnO, Fe-doped ZnO, and Fe–B co-doped ZnO thin films, Journal of Materials Science: Materials in Electronics 2024 35:17 35 (2024) 1136.
[20] P. Scherrer, Bestimmung, der Grosse und der inneren Struktur von Kolloidteilchen mittels Rontgenstrahlen. Nachrichten von der Gesellschaft der Wissenschaften zu Gottingen, Ges Wiss Göttingen 26 (1918) 98–100.
[21] M. Caglar, S. Ilican, Y. Caglar, F. Yakuphanoglu, Boron doped nanostructure ZnO films onto ITO substrate, J. Alloys Compd. 509 (2011) 3177–3182.
[22] B.J. Lokhande, P.S. Patil, M.D. Uplane, Studies on structural, optical and electrical properties of boron doped zinc oxide films prepared by spray pyrolysis technique, Physica B Condens. Matter 302–303 (2001) 59–63.
[23] Y. Ammaih, A. Lfakir, B. Hartiti, A. Ridah, P. Thevenin, M. Siadat, Structural, optical and electrical properties of ZnO:Al thin films for optoelectronic applications, Optical and Quantum Electronics 2013 46:1 46 (2013) 229–234.
[24] N. Nasiri, R. Bo, F. Wang, L. Fu, A. Tricoli, Ultraporous Electron-Depleted ZnO Nanoparticle Networks for Highly Sensitive Portable Visible-Blind UV Photodetectors, Advanced Materials 27 (2015) 4336–4343.
[25] A. Atılgan, K. Özel, Boron-Doped Thin Films Fabricated by the Spin Coating Method: The Effect of Doping Concentrations, Gazi University Journal of Science Part A: Engineering and Innovation 11 (2024) 57–67.
[26] G. Bagha, K. Samavati, H. Naffakh-Moosavy, L.F. Matin, Controlling surface morphology of Ag-doped ZnO as a buffer layer by dispersion engineering in planar perovskite solar cells, Scientific Reports 2024 14:1 14 (2024) 4617.
[27] D.K. Chaudhary, Y.S. Maharjan, S. Shrestha, S. Maharjan, S.P. Shrestha, L.P. Joshi, Sensing Performance of a ZnO-based Ammonia Sensor, Journal of Physical Science 33 (2022) 97-108.
[28] D. Garcia-Alonso, S.E. Potts, C.A.A. Van Helvoirt, M.A. Verheijen, W.M.M. Kessels, Atomic layer deposition of B-doped ZnO using triisopropyl borate as the boron precursor and comparison with Al-doped ZnO, J. Mater. Chem. C Mater. 3 (2015) 3095–3107.
[29] D. Zhao, S. Sathasivam, M. Wang, C.J. Carmalt, Transparent and conducting boron doped ZnO thin films grown by aerosol assisted chemical vapor deposition, RSC Adv. 12 (2022) 33049–33055.
[30] U.R. Dash, M.K.R. Khan, M.M. Rahman, M. Kamruzzaman, Effect of low to heavily boron doped pyrolized zinc oxide (ZnO:B) thin films, J. Phys. Conf. Ser. 1086 (2018) 012005.

© 2026 NSP
Natural Sciences Publishing Cor.